D-Watch: Embracing "bad" Multipaths for Device-Free Localization with COTS RFID Devices

Ju Wang[†], Jie Xiong[♯], Hongbo Jiang[‡], Xiaojiang Chen[†], Dingyi Fang[†]
[†]Northwest University; [♯]Singapore Management University;
[‡]Huazhong University of Science and Technology
[†]{wangju,xjchen,dyf}@nwu.edu.cn, [♯]jxiong@smu.edu.sg,[‡]hongbojiang2004@gmail.com

ABSTRACT

Device-free localization, which does not require any device attached to the target is playing a critical role in many applications such as intrusion detection, elderly monitoring, etc. This paper introduces D-Watch, a device-free system built on top of low cost commodity-off-the-shelf (COTS) RFID hardware. Unlike previous works which consider multipaths detrimental, D-Watch leverages the "bad" multipaths to provide a decimeter-level localization accuracy without offline training. D-Watch harnesses the angle-of-arrival (AoA) information from the RFID tags' backscatter signals. The key intuition is that whenever a target blocks a signal's propagation path, the signal power experiences a drop which can be accurately captured by the proposed novel P-MUSIC algorithm. The wireless phase calibration scheme proposed does not interrupt the ongoing communication. Real-world experiments demonstrate the effectiveness of D-Watch. In a rich-multipath library environment, D-Watch can localize a human target at a median accuracy of 16.5 cm. In a table area of 2 m×2 m, D-Watch can track a user's fist at a median accuracy of 5.8 cm. D-Watch is capable of localizing multiple targets which is well known to be challenging in passive localization.

Categories and Subject Descriptors

C.2.1 [**Computer-Communication Networks**]: Network Architecture and Design– *Wireless communication*

Keywords

Device-Free Localization; AoA; MUSIC; Multipath

CoNEXT'16, December 12-15, 2016, Irvine, CA, USA

DOI: http://dx.doi.org/10.1145/2999572.2999589

1. INTRODUCTION

While GPS localization has gained a huge success in outdoor environment, we witnessed an ever-increasing roll-out of indoor location-based applications such as shop navigation [31, 38], augmented reality [58, 20] and room occupancy detection [40] in recent years. Diverse technologies have been explored for localization purposes including infrared [21, 19], camera [28, 30], acoustic [14, 56], visible light [25, 26], Wi-Fi [53, 22, 23, 49], RFID [45, 45, 46, 55, 18], etc. Among all the technologies, radio frequency (RF)-based localization is considered most promising due to its ubiquitousness and low cost. In particular, RFID is evolving as a major candidate for identifying and tracking objects in indoor environment [13]. It is no exaggeration to say that we are almost surrounded by RFID tags in our daily lives. These tags are widely used in the bus cards, car keys, clothing security tags, etc. One main reason for this widespread deployment is the simplicity of the tags and the extremely low cost (each tag costs 5–10 cents USD).

The RF-based localization schemes can be further categorized into device-based [53, 22, 23, 45, 46, 52, 50] and device-free [47, 7, 8, 55, 49, 27]. The device-based schemes require the target to be equipped with a device or attached with a tag capable of emitting or reflecting RF signals. However, device-based localization is not applicable in some scenarios. In intruder detection, the targets will deliberately discard any device that can be tracked. In elderly care, old people are usually reluctant [55] to hold mobile devices, wear wearables or be attached with RFID tags. These real-life scenarios motive the needs of device-free localization which does not require any device to be attached to the target. On the other hand, device-free localization is usually more challenging as the weak reflected signals are employed for localization. For example, RFID adopts backscattering strategy for communication and the signal backscattered from the RFID tag is relatively weak. If the backscattered signal gets reflected again from the human target, it becomes extremely weak and it is difficult to retrieve this subtle signal for localization. Also multi-target tracking is not a problem for device-based

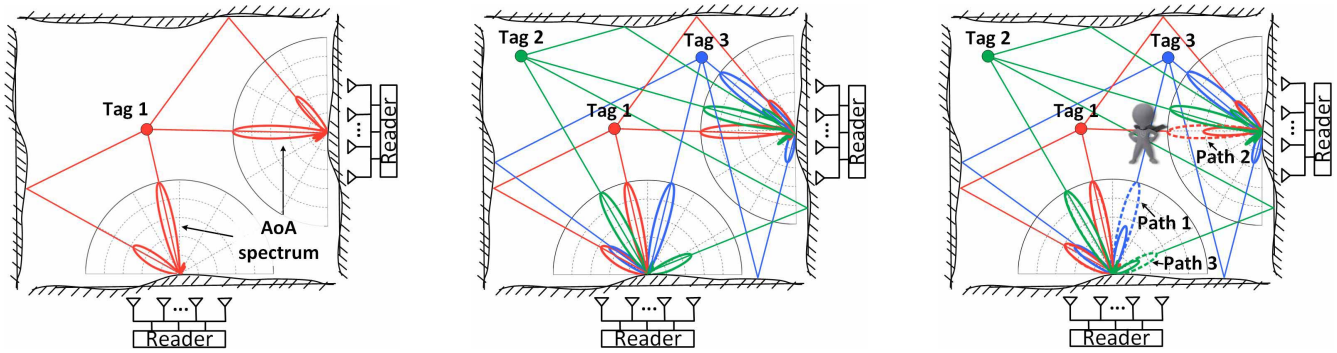

(a) One tag deployed. (b) Three tags deployed. (c) 3 paths are blocked by a target.

Figure 1: Illustration of the basic idea of D-Watch.

localization but becomes challenging for device-free systems as the reflected signals from multiple targets are all mixed together.

Most RF-based device-free systems [18, 10, 57, 49] employ the received signal strength indicator (RSSI) or channel state information (CSI) for localization which are coarse in accuracy and require labour intensive offline training to obtain the fingerprint database. The fingerprints also need to be updated if there are changes in the environment such as furniture movements, making these systems less realistic for real-life deployment. RSSI/CSI model-based schemes [33, 48, 54, 44] are proposed later to mitigate the fingerprint collection load but suffer from low accuracy in rich-multipath environments. In recent years, motivated by the radar array system [40, 53, 17], AoA-based schemes [8, 55, 47, 58] become popular with the opportunity of multiple antennas attached to a single Wi-Fi access point (AP) or an RFID reader. Wi-Fi APs nowadays are usually equipped with an antenna array due to the adoption of MIMO technology [24] in the latest 802.11n and 802.11ac standards. In order to increase the transmission range and accordingly the coverage area, the commodity RFID readers also have multiple antenna ports [46, 5]. The AoA-based schemes are able to achieve a high accuracy without labour intensive offline training. However, one major challenge for the success of AoA-based schemes is the identification of the LoS direct path. This is critical as there are usually rich multipaths indoors and only the direct path signal bouncing off the target contains the true angle information of the target. The multipaths are considered detrimental and several works [7, 8, 55] have been proposed to identify or remove these "bad" multipaths.

This paper introduces D-Watch, the first RFID-based device-free localization system that efficiently leverages the "bad" multipath signals to provide decimeter level accuracy. D-Watch is built on the COTS RFID hardware. To locate the target, D-Watch employs the AoA spectrum as shown in Fig. 1(a) and monitors the AoA peak changes to detect the angle information of the target. Specifically, if a target blocks a signal propagation path between the reader and the tag, the corresponding AoA peak will experience a drop. By monitoring the peak amplitude changes on the AoA spectrum, D-Watch can identify the target's angle information without any tag attached to the target, like a "direction-watcher (D-Watch)". We then combine the angle information from at least two non-collinear readers to localize the target by the triangulation method.

To further illustrate D-Watch's basic idea, Fig. 1 shows a toy example with two readers and three tags. We can see in Fig. 1(b) that the number of signal paths increases rapidly with two more tags added. When there is a human target in the area, D-Watch localizes the target as illustrated in Fig. 1(c). Specifically, multiple corresponding peaks on the AoA spectra are decreased when the target blocks path 1, path 2 and path 3. By rejecting the wrong angle from path 3 as we will discuss in Section 4.3, D-watch is able to localize the target with the other two paths.

D-Watch efficiently utilizes both the direct path and the reflection paths to identify the angle information of the target. With rich multipaths in indoor environment, D-Watch increases the coverage area significantly, so the deployment density can be well reduced. Further, D-Watch does not need to know the RFID tags' locations so the tags can be randomly placed with a high degree of flexibility. D-Watch only requires baseline AoA measurements between tags and readers, which take a few seconds compared with hours measuring and updating the RSS/CSI signatures at all possible locations in existing fingerprint-based location systems.

Though the basic idea sounds straightforward, it is non-trivial to realize D-Watch in practice due to the following challenges:

- **Phase calibration:** accurate AoA estimation is highly dependent on the signal's phase value measured at each antenna. However, each radio front end has a random phase offset introduced by the internal oscillator. This random phase offset needs to be carefully addressed before correct AoA information can be obtained. ArrayTrack [51] proposed a wired calibration method by injecting the same signals to the RF front ends with the help of a splitter. However, the wired calibration scheme

requires human intervention to plug/unplug the antennas which is time consuming and interrupts the ongoing communication.

- **Signal power estimation of each path:** the signal power of a certain path can not be estimated accurately with the well-known MUSIC algorithm [34] widely used for AoA estimation. The peak amplitude on an AoA spectrum estimated by MUSIC is a probability function [34] and does not have a clear linear relationship with the signal power. When one path is blocked, more than one peak on the MUSIC spectrum may get changed, resulting in a false positive detection. When multiple paths are blocked, MUSIC may only detect one path and miss the other blocked paths.

To deal with the above challenges, we propose a new wireless phase calibration scheme. Compared to the existing methods [51, 37], the proposed scheme does not interrupt the ongoing data communication and runs automatically without the requirement of human intervention. The basic idea is that the estimated AoA angle will match the true angle if the random phase offsets are removed correctly. By deploying tags with known direct path angles and treating the random phase offsets as unknowns, we can compose enough constraint equations to determine the random phase offsets.

We further propose a novel power MUSIC (P-MUSIC) algorithm, which reserves the AoA estimation capability of the traditional MUSIC and incorporates the signal power estimation capability so both the path angle and path signal power can be obtained at the same time. The key intuition behind P-MUSIC's power estimation is that it applies different weights to the signals received at each antenna so the desired signals at a specific direction add constructively, whereas the signals along other directions add randomly. This alignment boosts the power at the desired direction and averages out the signals along other directions to a small value so the signal power at a specific direction can then be estimated.

We build a prototype of D-Watch using four Impinj readers [5] and 21 Alien tags [1]. We evaluate the localization performance in three typical indoor environments: a library, a laboratory and an empty hall corresponding to high, medium and low multipath environment, respectively. D-Watch is able to achieve a median localization accuracy of 16.5 cm for a human target in the rich-multipath library environment. For a smaller scale deployment, D-Watch is able to perform fine-grained tracking of a user's fist passively at a median accuracy of 5.8 cm. D-Watch also moves one step further to localize multiple targets simultaneously which is well known to be challenging for passive localization. D-Watch is able to localize three glass bottles at the same time at a maximum error of 17.2 cm as long as they are separated by at least 20 cm from each other.

Contributions: The main contributions of this paper are summarized as follows:

- D-Watch is the first device-free RFID system that efficiently utilizes the "bad" multipaths for localization. D-Watch does not require labour intensive offline training nor needs to know the RFID tags' locations, making D-Watch a promising candidate for real life large scale deployments.
- The proposed wireless phase calibration scheme operates without reliance on human intervention. It outperforms the state-of-the-art wireless calibration method and does not interrupt the ongoing communication.
- We propose a novel P-MUSIC algorithm, which does not only capture the angle information as the traditional MUSIC algorithm does but also obtains the signal power information of each path.
- D-Watch is implemented on COTS RFID hardware and comprehensive experiments demonstrate the effectiveness of the system. D-Watch can be easily extended to Wi-Fi and other RF-based systems for localization and tracking purposes.

Paper outline: We introduce the background and challenges in Section 2 and Section 3. We detail D-Watch's design in Section 4. The implementation is described in Section 5 followed by the evaluation in Section 6. The related work is in Section 7. We discuss some related issues in Section 8 and conclude our work in Section 9.

2. BACKGROUND

In this section, we introduce the technical background of RFID and MUSIC algorithm.

2.1 RFID System

An RFID system usually consists of a reader and multiple tags. Tags have no internal battery, so they harvest energy purely from the reader's signal and reply to the reader with a modulated backscatter signal. Typically, a COTS reader is connected to multiple antennas to increase the coverage range. For example, the Impinj xArray reader [5] has 52 antennas and covers more than 139 m^2 space with a price of 2000 USD.

Two points about RFID system are particularly relevant to the device-free localization. First, an RFID tag is extremely cheap at a cost of 5–10 cents USD. RFID reader is relatively expensive (the price [2] of the ThingMagic reader is around 450 USD and the general purpose Impinj R420 reader is around 1200 USD). R420 is relatively expensive because of the HTTP/TCP server function which is not used in our localization system. One R420 reader has four RF port and is capable of being connected to multiple antennas serving many RFID tags so the price is well amortized. RFID-based localization system is thus a promising candidate for large-scale deployments in cargo transportation, retailing and warehouse. Second, the communication range of RFID today is significantly increased to more than 10 meters [5, 45]. Major RFID manufacturers are competing to increase the range [46] and we expect the range

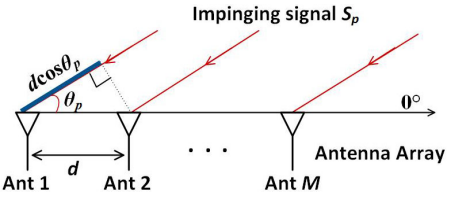

Figure 2: Phase changes are different when a signal arrives at different antennas of a linear array.

to continue growing in the next few years.

2.2 AoA and MUSIC

AoA information. When an RF signal propagates in the air, the phase keeps rotating and one wavelength of distance corresponds to a 2π phase rotation. The basic idea of AoA estimation is to measure the signal phase difference at antennas [32] due to different propagation distances. For example in Fig. 2, the adjacent antennas are placed with a space of $d = \lambda/2$ in between, where λ is wavelength. A signal arrives at the antennas along direction θ_p. If the phase measurements at the first two antennas are ϕ_1 and ϕ_2, we can then estimate the AoA θ_p as:

$$\theta_p = \arccos(\frac{\lambda \cdot |\phi_1 - \phi_2|}{2\pi \cdot d}) = \arccos(\frac{|\phi_1 - \phi_2|}{\pi}). \quad (1)$$

AoA estimation by MUSIC. In reality, Equation (1) does not work because of the multipath signals. MUSIC [34] algorithm is employed for multipath signal AoA estimation. Consider a uniform linear array with M antennas where the first antenna is taken as the reference antenna as shown in Fig. 2. P signals S =[s_1, s_2, $\cdots$, s_P]^T arrive at the array at directions of Θ=[θ_1, θ_2, $\cdots$, θ_P]. Since the signals are all mixed, the measured signal x_m at "antenna m" can be expressed as:

$$x_m = \sum_{p=1}^{P} s_p \cdot e^{-j\cdot\omega(m,\theta_p)}, \quad (2)$$

where $\omega(m,\theta_p)$=$(m-1)\frac{2\pi d}{\lambda}cos(\theta_p)$. The measured signal vector $\mathbf{X} = [x_1, x_2, \cdots, x_M]^T$ at the array is:

$$\mathbf{X} = \mathbf{AS} + \mathbf{n}, \quad (3)$$

where $\mathbf{n}$ is noise, $\mathbf{A}$=[$\mathbf{a}(\theta_1)$, $\cdots$, $\mathbf{a}(\theta_p)$, $\cdots$, $\mathbf{a}(\theta_P)$] is the steering matrix and $\mathbf{a}(\theta_p)$ is an $M \times 1$ steering vector:

$$\mathbf{a}(\theta_p) = [1, e^{-j\cdot\omega(2,\theta_p)}, \cdots, e^{-j\cdot\omega(M,\theta_p)}]^T, \quad (4)$$

where $(\cdot)^T$ denotes the transpose operation.

MUSIC is based on eigenstructure analysis of the signal vector's correlation matrix $\mathbf{R}$. Based on (3), the correlation matrix $\mathbf{R}$ can be expressed as:

$$\mathbf{R} = \mathbb{E}[\mathbf{X}\mathbf{X}^H] = \mathbf{A}\mathbb{E}[\mathbf{S}\mathbf{S}^H]\mathbf{A}^H + \sigma^2\mathbf{I}, \quad (5)$$

where $(\cdot)^H$ denotes the Hermitian transpose operation, $\mathbb{E}[\mathbf{S}\mathbf{S}^H]$ is the source correlation matrix. The array correlation matrix $\mathbf{R}$ has M eigenvalues λ_1,$\cdots$,λ_M associated with M eigenvectors $\mathbf{U}$=[$\mathbf{u}_1$, $\cdots$, $\mathbf{u}_M$]. The largest P eigenvalues correspond to the P incoming signals while the rest Q= $M-P$ correspond to the noise. We choose P value based on how many eigenvalues are larger than a threshold and considered signals. Based on this process, the corresponding eigenvectors in $\mathbf{U}$ can be classified as signal and noise parts:

$$\mathbf{U} = [\mathbf{U}_S, \mathbf{U}_N] = [\underbrace{\mathbf{u}_1, \cdots, \mathbf{u}_P}_{\mathbf{U}_S}, \underbrace{\mathbf{u}_{P+1}, \cdots, \mathbf{u}_M}_{\mathbf{U}_N}]. \quad (6)$$

We refer to $\mathbf{U}_S$ as the *signal subspace* and $\mathbf{U}_N$ as the *noise subspace*. Due to the orthogonality between the signal steering vector and noise subspace [34], we have:

$$\mathbf{a}(\theta)^H\mathbf{U}_N = \mathbf{0}, \quad (7)$$

when $\theta = \theta_1, \cdots, \theta_P$. Accordingly, the AoA spectrum of MUSIC is given as:

$$B(\theta_p)=\frac{1}{\mathbf{a}^H(\theta_p)\mathbf{U}_N\mathbf{U}_N^H\mathbf{a}(\theta_p)}, \quad (8)$$

which yields sharp peaks at the each signal's AoA.

3. CHALLENGE AND VERIFICATION

We discuss the challenges in detail and employ benchmark experiments to validate our claims in this section.

3.1 Phase Calibration

Accurate AoA estimations are the key part of our localization system. The AoA estimations are highly dependent on the accurate phase measurements. However, a reader's RF front ends introduce random phase offsets into the phase measurements. To examine the amount of phase offsets introduced, we conduct an empirical study over the 16 RF ports on four Impinj R420 readers, with 4 RF ports on each reader. We deploy one tag and one antenna with clear LoS path. The antenna is connected to the 16 RF ports via a same RF cable one by one and the phase measurements are recorded. We select the first RF port as the reference and calculate the phase offsets for the other 15 RF ports. Fig. 3 shows the measured phase offsets ranging from $-85.9°$ to $176°$. These offsets are very random and need to be removed in order to achieve reliable AoA estimates. Traditional calibration methods, such as ArrayTrack [51], Argos [37] and Phaser [17], though being able to obtain the phase offsets, require human intervention and take minutes to complete. What is worse, these methods interrupt the ongoing data communication.

3.2 Limitation of Power Estimation

D-Watch detects the target's direction by observing an obvious signal power reduction when the target blocks the signal path. Thus, an accurate path power change detection is critical for D-Watch's localization. However, the signal power of each path can not be estimated accurately with the well-known MUSIC algorithm [35]. The AoA spectrum estimated by MUSIC is a probability function [34] and the peak amplitude does not

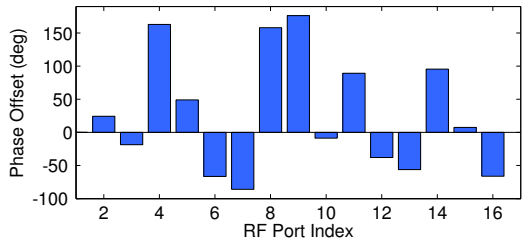

Figure 3: Random phase offsets at different RF ports.

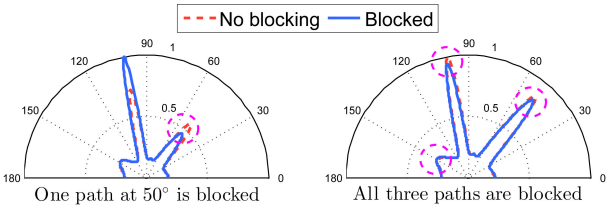

Figure 4: AoA spectrum change estimated by MUSIC.

represent the signal power level. We run a benchmark experiment to verify this observation and show the results in Fig. 4. When one path at 50° is blocked, not just the peak of the blocked path is decreased, the peak amplitudes of other paths may also get changed. That is to say, the power information provided by traditional MUSIC is not reliable for target detection. What is worse, when all three paths are blocked, the amplitudes for all peaks do not change much on the spectrum as shown in Fig. 4. MUSIC will then miss some of the blocked paths and the targets may not even be detected.

4. SYSTEM DESIGN

We present the key components of D-Watch followed by a summary of the system workflow.

4.1 Wireless Phase Calibration

We propose a subspace based wireless calibration method to estimate the phase offsets without interrupting the ongoing communication. The main challenge faced by wireless calibration is the multipath effect. With different propagation paths, the signals combine constructively at some antennas while combine destructively at other antennas. A naive approach is to remove the multipath signals so that we get the phase measurements only caused by the direct path signal and the RF port phase offsets. We can then obtain the phase offsets because the phase difference introduced by the direct path signal can be calculated. However, in a typical indoor environment, multipaths exist and it's difficult to remove the multipath signals from the received mixed signal and only keep the direct path signal.

In contrast, we propose a novel method which is able to work in the presence of multipath signals. The key intuition is the orthogonality property between the signal subspace and noise subspace, if we carry out eigenvalue analysis on the signal correlation matrix [34] as we described in Section 2.2. Based on this orthogonality property, the product of the noise subspace and signal subspace approaches zero at the LoS angle when the phase offsets are correctly removed. This observation motivates us to find the phase offsets by minimizing the product of noise and signal subspace at the known LoS angle[1]. With phase offsets, we revise the array signal model described by (2) as:

$$\mathbf{X} = \Gamma \mathbf{A} \mathbf{S} + \mathbf{n}, \tag{9}$$

where $\mathbf{X}$, $\mathbf{A}$, $\mathbf{S}$ and $\mathbf{n}$ are the array signal vector, steering matrix, source signal and noise. $\Gamma = \text{diag}\{1, e^{j\cdot\Delta\beta_{2,1}}, \cdots, e^{j\cdot\Delta\beta_{M,1}}\}$ is the phase offset diagonal matrix. $\Delta\beta_{m,1} = \beta_m - \beta_1$ refers to the phase offset between "antenna m" and the reference "antenna 1". From Equation (7), we have $\mathbf{a}(\theta)^H \Gamma^H \mathbf{U}_N = \mathbf{0}$ at $\theta = \theta_1, \cdots, \theta_P$. We then estimate the unknown hardware phase offset matrix $\hat{\Gamma}$ by solving the equation $||\mathbf{a}(\theta)^H \Gamma^H \mathbf{U}_N||_{l_2}^2 = 0$ with the angle θ and the noise eigenvector $\mathbf{U}_N$ known. The direct path angle $\theta_{LoS}^{(k)}$ of the k^{th} tag can be easily measured when the locations of the tags and antennas are known[2]. The estimation accuracy of $\hat{\Gamma}$ can be further improved with larger number of tags. Thus, a more general equation can be given as:

$$\sum_{k=1}^{K} \left\| \mathbf{a}(\theta_{LoS}^{(k)})^H \Gamma^H \mathbf{U}_N^{(k)} \right\|_{l_2}^2 = 0, \tag{10}$$

where K is the total number of tags. Note that the dimensions of $\mathbf{a}(\cdot)$, Γ and $\mathbf{U}_N$ are $1 \times M$, $M \times M$ and $M \times (M-P)$, respectively. By expanding Equation (10), we acquire a number of $K \times (M-P)$ sub-equations. In practice, the number of dominant paths P for indoor environments is no larger than five [51]. Thus, we have more than $K(M-5)$ equations. While $K(M-5)$ grows in a quadratic fashion, the number of unknown phase offsets $M-1$ grows linearly. This suggests that given enough number of tags, there are enough ($K(M-5) \geq M-1$) equations to determine the unknown $\hat{\Gamma}$.

There are several approaches to solve a set of over-determined equations such as inverting the equations directly or applying the least squares method. However, these approaches are not efficient in solving our problem due to a large amount of non-linear exponential terms in the equations. In this paper, we formulate an optimization problem to find $\hat{\Gamma}$ that minimizing:

$$\hat{\Gamma} = \underset{\Gamma}{\text{argmin}} \sum_{k=1}^{K} \left\| \mathbf{a}(\theta_{LOS}^{(k)})^H \Gamma^H \mathbf{U}_N^{(k)} \right\|_{l_2}^2. \tag{11}$$

The above optimization problem can be solved effectively applying a hybrid method of genetic algorithm (GA) [29] and gradient descent (GD) [9]. Specifically, in each iteration, GA starts initiating all the unknowns

[1]To make sure the LoS path dominates, we place the receiver close to the transmitter with clear LoS path.
[2]The tags' locations are only required for phase calibration. We do not need the tags' locations in localization.

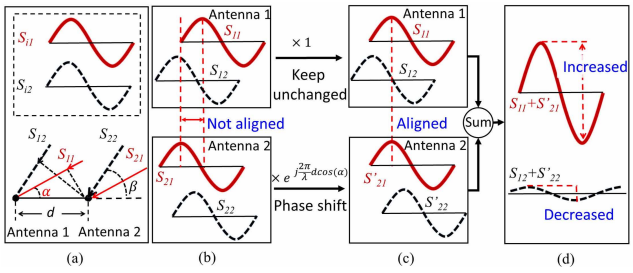

Figure 5: Illustration of obtaining the desired signal at one particular direction with alignment and summation.

and then refines the solution with the GD algorithm to find the closest local minimum.

4.2 Power MUSIC

We introduce a power MUSIC (P-MUSIC) algorithm to address the issue of missing power information in traditional MUSIC algorithm. The key observations are:

- The mixed signal received at one antenna is different from that received at another antenna due to the propagation path difference of signals.
- For a signal at one direction, the phase difference at any two adjacent antennas is the same and can be easily calculated.
- Different phase weights can be applied to the measured signals at different antennas so the signals at a designed direction add constructively, whereas the signals along other directions randomly add. This alignment boosts the power at the desired direction and averages out the signals at other directions to a small value, so the signal power at the designed direction can be obtained.

Fig. 5 (a) shows a toy example with two antennas spaced at a distance of d. Two signals arrive at two different angles α and β. We donate the two signals as S_{i1} and S_{i2} when they reach "antenna i". The two signals are mixed together at each antenna. To obtain the signal power at angle α, we apply two carefully chosen weights $[1, e^{j\frac{2\pi}{\lambda}d\cos(\alpha)}]$ to the measured signals and then sum them up. S_{11} and S'_{21} then add up constructively, while the other signals add up destructively, as shown in Fig. 5 (d). With the alignment and summation, we successfully reduce the power in other angles and obtain the power at angle α. Note that with just two antennas, the other signals may still have a chance of adding up constructively. However, with more antennas, other signals add up with random phase shifts, which will average out to a small value.

Without loss of generality, assume we want to identify the signal power s_1 along direction θ_1. The measured signal at "antenna m" is x_m. Then the sum of the weighted versions of x_m at direction θ_1 is given as:

$$\begin{aligned}
&\sum_{m=1}^{M} x_m \cdot e^{j\cdot\omega(m,\theta_1)} \\
&= \left(s_1 + \sum_{p=2}^{P} s_p\right) + \left(s_1 + \sum_{p=2}^{P} s_p \cdot e^{-j\cdot[\omega(2,\theta_p)-\omega(2,\theta_1)]}\right) \\
&+ \cdots + \left(s_1 + \sum_{p=2}^{P} s_p \cdot e^{-j\cdot[\omega(M,\theta_p)-\omega(M,\theta_1)]}\right) \\
&= M\cdot s_1 + \sum_{p=2}^{P}\left[s_p\left(\sum_{m=1}^{M} e^{-j\frac{2\pi(m-1)d}{\lambda}[\cos(\theta_p)-\cos(\theta_1)]}\right)\right]
\end{aligned} \tag{12}$$

As shown in the above equation, the signal s_1 adds constructively and the amplitude gets increased roughly M times while other signals average out when adding up with random phase shifts of $\frac{2\pi(m-1)d}{\lambda}\cos(\theta_p)$. For any interested signal s_p, with the alignment and summation, the power of the designed signal along direction θ_p will be much higher than the power along other directions with a relatively large M. The signal power along the direction θ_p with the received signals at the M antennas is then given as:

$$P_B(\theta_p) = \|s_p\|^2 \approx \frac{\left\|\sum_{m=1}^{M} x_m \cdot e^{j\cdot\omega(m,\theta_p)}\right\|^2}{M^2}. \tag{13}$$

We then integrate this power information into the traditional MUSIC to acquire both AoA and power estimations. Intuitively, we can simply dot-multiply the power estimation $P_B(\theta_p)$ and the MUSIC AoA spectrum $B(\theta_p)$. However, the MUSIC peak amplitude is a probability value, which distorts the estimated signal power. We solve this problem by designing a normalization function $Nor(B(\theta_p))$ to normalize all the peak amplitudes to "1". We thus remove the peak amplitudes from MUSIC and only keep the angle information of the peaks. Our P-MUSIC function is then given as below:

$$\begin{aligned}
\Omega(\theta_p) &= P_B(\theta_p)\cdot Nor(B(\theta_p)) \\
&= \frac{\left\|\sum_{m=1}^{M} x_m\cdot e^{j\cdot\omega(m,\theta_p)}\right\|^2}{M^2\cdot Nor(\mathbf{a}^H(\theta_p)\mathbf{U}_N\mathbf{U}_N^H\mathbf{a}(\theta_p))},
\end{aligned} \tag{14}$$

where M is the number of antennas, $\mathbf{a}(\theta_p)$ and $\mathbf{U}_N$ are the steering vector and the noise subspace eigenvector defined in Section 2.2.

Note that P-MUSIC does not need to know the value of θ_p. By searching θ_p from 0 to π like the traditional MUSIC, P-MUSIC is able to estimate the signal power along each direction of the signal path. The coherence between signals affects the performance of P-MUSIC and we adopt the spatial smoothing method [36] to remove the coherence among received signals.

4.3 Target Localization

D-Watch combines the identified target angles from several readers to determine the target's location. Suppose ξ readers identify a set of AoA spectra changes $\Delta\Omega_1(\theta), \cdots, \Delta\Omega_\xi(\theta)$. To localize a target, we compute the likelihood function $L(O)$ of the target be located

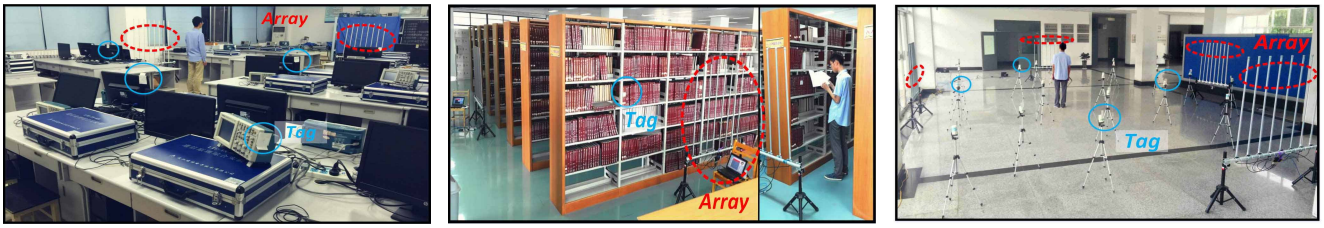

(a) Laboratory environment. (b) Library environment. (c) Hall environment.

Figure 6: Three typical indoor environments corresponding to medium, high and low multipath environment.

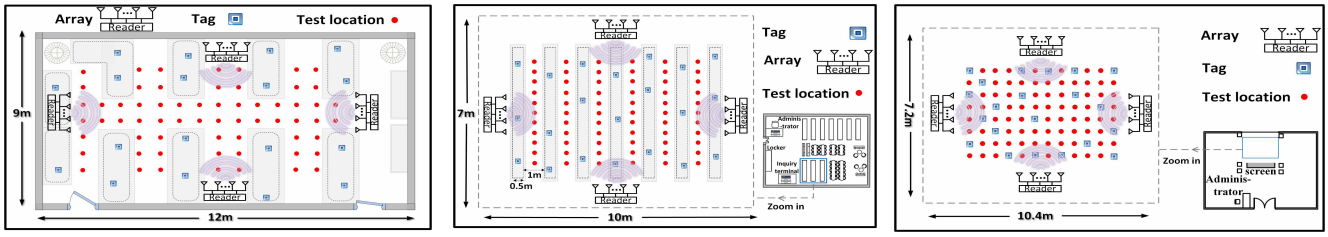

(a) Laboratory deployment layout. (b) Library deployment layout. (c) Hall deployment layout.

Figure 7: Deployment layouts with the positions of arrays, tags and test locations marked.

at a position O, and take the location estimate with a maximum likelihood as the target location. To compute the likelihood, the basic idea is that a larger AoA peak change indicates a higher probability that the target is at this angle. The likelihood $L(O)$ is given as:

$$L(O) = \prod_{i=1}^{\xi} \Delta\Omega_i(\theta). \quad (15)$$

We then divide the monitoring area into grids[3] and search for the grid with the highest $L(O)$. The hill climbing scheme is employed to quickly find the most likely target location estimate.

Note that we may retrieve wrong angle information if the target blocks a reflection path before the signal reaches the reflector. In Fig. 1(b), Path 3 is blocked but the angle information detected is not correct. In reality, this wrong angle information can be identified if there is only one target. Because a target cannot block two paths at the same reader at the same time. Whenever we detect multiple blocked paths at one reader, we know only one of the detected angles is pointing to the true location of the target. We further discover that the locations estimated from the wrong angles are distributed at random positions and even far outside of the monitoring area. On the other hand, the correct angles will localize the target to close-by positions. We can then apply outlier rejection to identify the wrong angle.

4.4 Putting Things Together

Now we put all the pieces together and sketch the workflow of D-Watch.

[3]Smaller grid size leads to more accurate results but takes more time to search. We balance this tradeoff and set the grid size as 5 cm×5 cm for the three indoor environments and 2 cm×2 cm for the smaller table area.

Step 1: Data collection. D-Watch collects a set of baseline AoA data between the tags and the reader when no target is present. Note that this process is very different from the traditional fingerprint database collection which takes hours. This process for D-Watch is just several transmissions between the readers and tags which can be well completed within seconds. D-Watch then acquires another set of measurements when the target moves into the monitoring area.

Step 2: Data pre-processing. D-Watch first employs the proposed wireless phase calibration method to remove the phase offsets that exist in the collected data. Note that the calibration process is a one-time effort for one power on-off cycle so D-Watch does not need to carry out phase calibration frequently.

Step 3: Target angle estimation. With proposed P-MUSIC algorithm, D-Watch generates two sets of AoA spectra based on the online data and the baseline data. By comparing the amplitude changes of the AoA peaks, D-Watch can accurately identify the target's angle information at each reader.

Step 4: Target localization. By combining the identified angle information from multiple readers, D-Watch is able to obtain the target's location estimate with triangulation scheme.

5. IMPLEMENTATION

Experimental environments: we conduct experiments in three typical indoor environments: a library, a laboratory and an empty hall corresponding to high, medium and low multipath environment. The laboratory with a size of 9 m×12 m has many small objects such as test chambers, displays, etc., as shown in Fig. 6(a). Part of the library area with a size of 7 m×10 m has many book shelves full of books, as shown in Fig. 6(b). The shelf has a height of 2.5 m

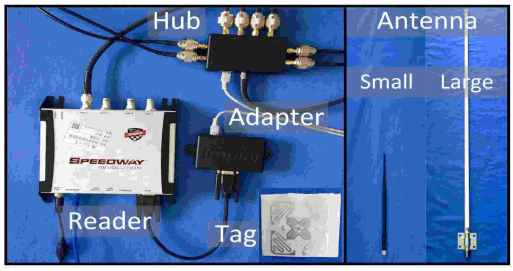

Figure 8: RFID hardware and antennas employed.

and is made of metal and wood, resulting in rich multipaths and strong NLoS. Part of the empty hall with a size of 7.2 m×10.4 m is shown in Fig. 6(c).

Human target and object target: We ask the students to act as the human target in the experiments. To demonstrate the high accuracy of D-Watch in a small scale deployment, we employ three glass bottles full of water as our object targets. The bottle has a bottom diameter of 7.8 cm and a height of 22 cm.

Implementation: (i) *Readers and tags.* We employ four Impinj Speedway R420 readers [5] for our experiments without any hardware or firmware modification. Each reader has four RF ports and is equipped with one Impinj GPIO Adapter [5]. An Impinj antenna hub is connected to one of the reader's four RF ports as shown in Fig. 8. Usually, we need 8 antennas for high accuracy AoA estimation [51]. However, the Impinj Speedway R420 reader only has four antenna ports, thus we use the antenna hub provided by Impinj to support more antennas. The readers are compatible with EPC Gen2 standard [4] and the antennas work in a time division multiplexing mode. The time slot for each antenna is about 200 us [5]. The reader operates in frequency range of 920.5–924.5 MHz, which is the legal UHF band in China. We use 21 cheap Alien ALN-9634 tags [32] as shown in Fig. 8, which cost 1.5 USD in total.

(ii) *Antenna and array.* We employ two different types of antennas for our experiments as shown in Fig. 8. The small one is ANS-900 omni-directional antenna [3] and the large one is Q900F-900 omni-directional antenna [6]. Since RFID devices communicate by backscattering the signal which is usually weak, the small antenna [3] provides a relatively small communication range of 3 m. The large antenna provides a communication range of 12 m. Each linear array is consisted of 8 antennas with a half wavelength space of 16.25 cm between adjacent antennas. The antennas and the RF front ends have been calibrated using the wireless phase calibration method introduced in Section 4.1.

(iii) *Server and algorithm implementation*: The proposed schemes and algorithms are implemented in C# and Matlab. The server is a desktop with 3.6 GHz CPU (Intel i7-4790) and 8 GB memory. The server communicates with the RFID readers using low level reader protocol (LLRP) [15]. All the tags' backscatter packets received at the readers are forwarded to the server through Ethernet cables. The size of a RFID backscatter packet is small since the packet only contains the tag's ID which is 12 bytes at most [5]. The reader does not need to emit signals all the time and a 0.1 s transmission interval is good enough for our localization and does not increase the transmission overheads.

Default deployment setup: The deployment layouts of the three environments are shown in Fig. 7. In each environment, we deploy four[4] readers and 21 tags. The locations of the readers are known while the tags are randomly placed without a need to know their locations. We choose 63, 66 and 75 test locations in the laboratory, library and hall, respectively. The test locations are uniformly distributed with a 0.5 m distance in between. The objects attached with tags are usually placed on the table or held in the hand so their heights are between 1 to 1.5 m above the ground. We place the antenna array at a height of 1.25 m. When we evaluate the impact of number of tags and tag-array height difference, we employ more tags and change the default setup. Unless specifically mentioned, we use the default setup for performance evaluation.

Experimental methodology: When a target moves into the monitoring area, the readers receive 10 backscatter packets from each tag and forward them to the server. At the server side, D-Watch identifies the angle information of the target at each reader and combines the information from several readers to obtain the target's location estimate. We repeat the experiments 40 times at each test location.

6. PERFORMANCE EVALUATION

6.1 Microbenchmark

We start with two benchmark experiments to validate the effectiveness of the proposed wireless calibration method and P-MUSIC algorithm.

6.1.1 Verification of phase calibration method

We measure the random phase offsets caused by the reader's radio front ends and compare our method with the state-of-the-art wireless calibration method proposed in Phaser [17]. We take the phase offsets obtained from the wired calibration method proposed in ArrayTrack [51] as the ground truth. In the laboratory environment, tags are randomly attached to objects located 1–8 m away from the array. We vary the number of tags to estimate the phase offset matrix $\hat{\Gamma}$. The phase offset estimation errors are shown in Fig. 9. The proposed method is able to achieve phase error less than 0.05 radians when more than four tags are employed. It suggests that the proposed method achieves a high calibration accuracy even with a relatively small number of tags. Note that a phase calibration error of 0.05 radians will cause an even smaller AoA error since there

[4]Note that the number of readers can be reduced to one if we employ coaxial cables to connect four antenna arrays to one reader.

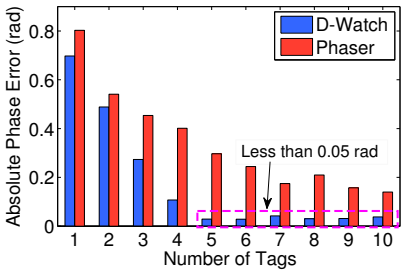

Figure 9: The proposed phase calibration method is much more accurate.

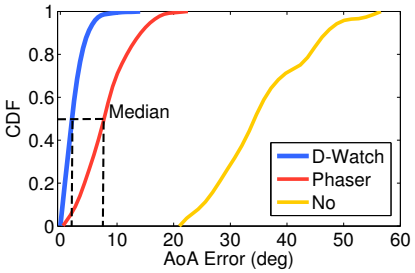

Figure 10: LoS AoA estimation with proposed calibration method.

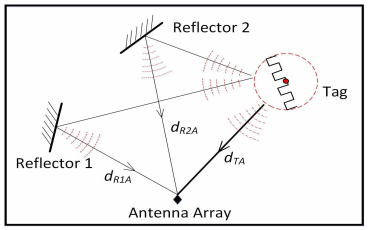

Figure 11: Deployment layout for Power MUSIC verification.

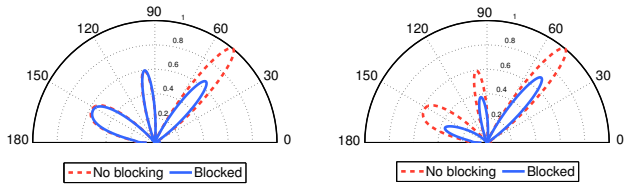

(a) One path is blocked. (b) Three paths are blocked.

Figure 12: AoA spectrum changes estimated by P-MUSIC when one or more paths are blocked.

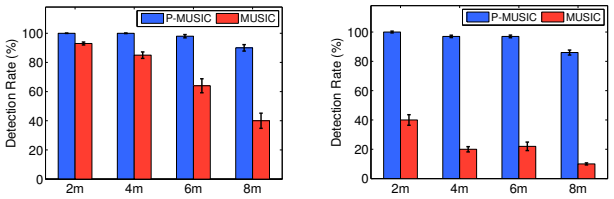

(a) One path is blocked. (b) All paths are blocked.

Figure 13: Target detection rate comparison between MUSIC and P-MUSIC.

are multiple antennas and the calibration errors have positive and negative values which may cancel out each other. We then compare the direct path AoA estimation errors when employing different calibration methods. The results in Fig. 10 show that our calibration method achieves a high AoA estimation accuracy, i.e., a median error of 2°, outperforming the Phaser system.

6.1.2 *Verification of power MUSIC*

To minimize the influence of multipath, we conduct this experiment in the empty hall environment. We place two laptops with metal shells as reflectors to obtain two controlled reflection signals. The deployment layout is shown in Fig. 11. Three human targets walk around to block the direct path and reflection paths. We increase the distance d_{TA} between the tag and the array from 2 m to 9 m, while keep the distances (i.e., d_{R_1A}=2 m and d_{R_2A}=2.6 m) from the two reflectors to the array unchanged. For the same distance, we also change the locations of the tag and the reflectors to have multiple measurements. To detect the presence of targets, we compare the changes of AoA peaks when there is no target and when targets are present.

Fig. 12 illustrates the changes of AoA spectra when we apply P-MUSIC. Compared with traditional MUSIC shown in Fig. 4, the changes of the AoA peaks estimated by P-MUSIC match our expectations, i.e., the blocked path peak experiences a clear drop and the unblocked peaks remain unchanged. The detection rate of P-MUSIC is close to 100% as shown in Fig. 13. On the other hand, the detection performance of traditional MUSIC is poor even when the signal strength is strong. Traditional MUSIC fails when multiple targets are present and block more than one paths at the same time. The proposed P-MUSIC is able to capture the power changes of each path much more accurately than the traditional MUSIC.

6.2 Overall Localization Performance

In reality, human target is too big to be treated as a point. As the human targets have a width of 32 cm to 40 cm, we consider there is no localization error as long as the estimation is within the 36 cm range. Otherwise, we calculate the error as the minimum difference between the estimated location and this 36 cm range.

We show the localization performance for the human target in three different environments in Fig. 14. The results in Fig. 14 (a) show that D-Watch achieves the best performance in the library environment with a median and 90% error as small as 16.5 cm and 28.9 cm, respectively. D-Watch's median accuracy slightly decreases in laboratory and hall environments to 25.3 cm and 32.1 cm. The mean errors are shown in Fig. 14 (b). The results are interesting as indoor localization systems usually achieve worse performance in richer multipath environments. In contrast, D-Watch performs even better, implying that "bad" multipaths are efficiently utilized to improve the localization performance.

6.3 Impact of Number of Antennas

We show the performance of D-Watch with varying number of antennas at the reader. In general, with more antennas at each reader, D-Watch is able to achieve a finer resolution in AoA estimation and capture more

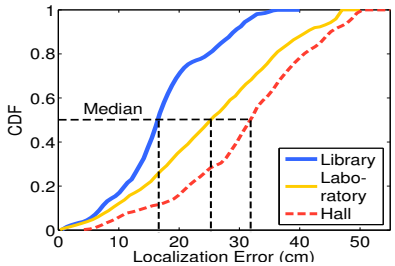

(a) CDF plot localization error.

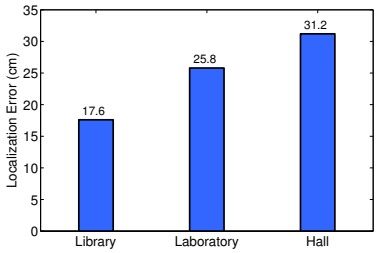

(b) Mean localization error.

Figure 14: Localization performance in different environments.

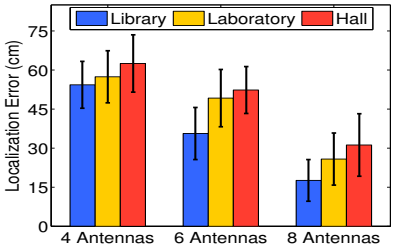

Figure 15: Localization errors with varying number of antennas.

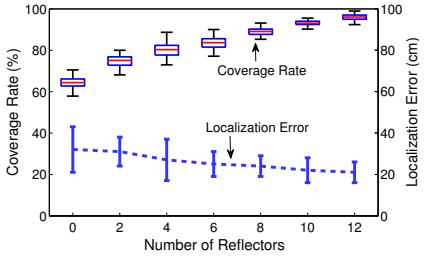

Figure 16: Localization errors with varying number of reflectors.

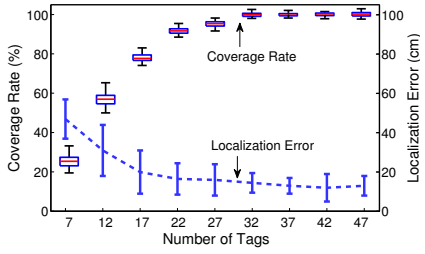

Figure 17: Localization errors with varying number of tags.

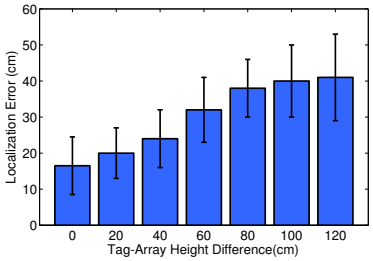

Figure 18: Localization errors with varying tag-array height differences.

paths, which accordingly increases the localization accuracy as shown in Figure 15. In the library environment, the mean localization error is 54.3 cm for four antennas, 35.6 cm for six antennas and 17.6 cm for eight antennas.

6.4 Impact of Number of Multipaths

Besides the direct path, D-Watch utilizes the multipaths to localize a target. With more multipaths, D-Watch achieves a higher coverage rate[5] and improves the localization accuracy. To demonstrate this, we place up to 12 reflectors such as laptops and metal reflectors to create more multipaths in the hall environment. Fig. 16 shows that the coverage rate gets increased significantly since more propagation paths exist in the monitoring area. It also shows a mean error decrease from 31.2 cm to 20.8 cm as more paths are now restricting the target's location estimate.

6.5 Impact of Number of Tags

With more tags, more signals will be reflected creating more paths to cover the monitoring area and constraint the target's location. In the library environment, we vary the number of tags from 7 to 47 with a step size of 5. The experimental results match our expectations as shown in Fig. 17. So both the number of tags and reflectors can actually increase the multipaths in the environment. Thus, in an indoor environment with more reflectors, the density of the tags can then be reduced.

Note that, more tags are helpful for improving the localization accuracy. However, the localization accuracy of D-Watch is mainly related to the AoA estimation accuracy so the number of antennas at the reader side is the main factor deciding the localization accuracy.

[5]Coverage rate is defined as the number of locations can be localized divided by total number of test locations.

6.6 Impact of Tag-Array Height Difference

In reality, tags attached on books or laptops are placed on the table or held in the hand with a height of 1–1.5 m above the ground. If the tags and the arrays are not at the same height, we would like to study whether such a height difference will cause significant localization errors. Fig. 18 shows that D-Watch can still achieve a mean localization error of 40 cm even when the height difference is as large as 120 cm. When the height difference is 40 cm, the mean error is 24 cm which is only slightly higher.

6.7 Multi-Target Localization

The high spatial resolution of D-Watch's AoA spectrum enables a fine-grained multi-target localization. The intuition is that a target is not able to block all the paths simultaneously. When multiple targets are located sparsely, each target will block a disjoint subset of paths and thus can be separated and individually located. However, when many targets exist or two targets are too close to each other, it's still challenging to accurately localize each of them.

We study the performance of D-Watch for multi-target localization. To evaluate the granularity of multi-target localization, we employ three glass bottles placed on a 2 m×2 m table as shown in Fig. 20. The bottles are filled with water. We place two small-antenna arrays at the midpoint of the bottom and right of the table. 26 tags are placed at the other two sides. Fig. 19 (a)∼(c) shows three snapshot localization results when the three targets are separated roughly by 130 cm, 50 cm and

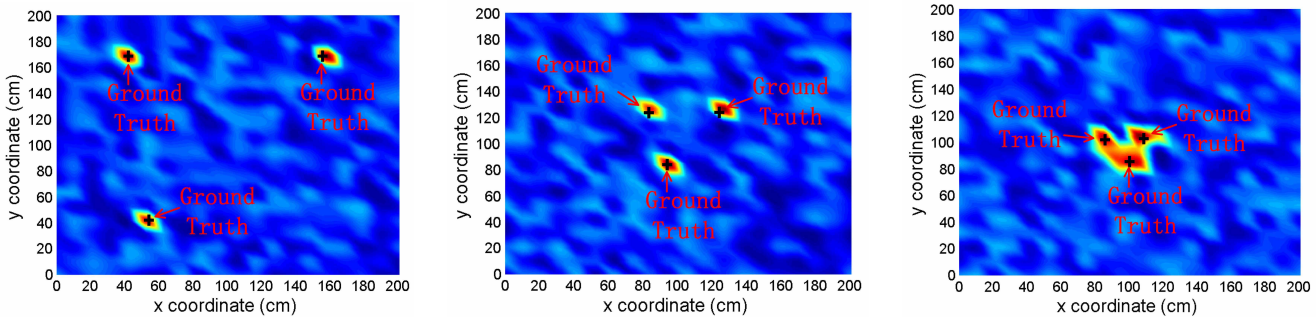

(a) Targets are 130cm apart. (b) Targets are 50cm apart. (c) Targets are 20cm apart.

Figure 19: Performance of multi-target localization. (a)-(c) show the heatmaps of three snapshot localization results.

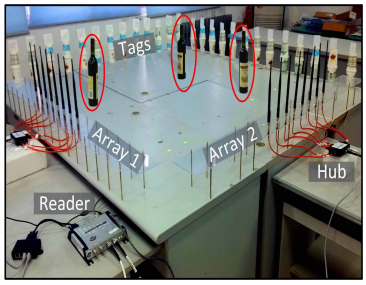

Figure 20: A 2 m × 2 m table area with three glass bottle targets.

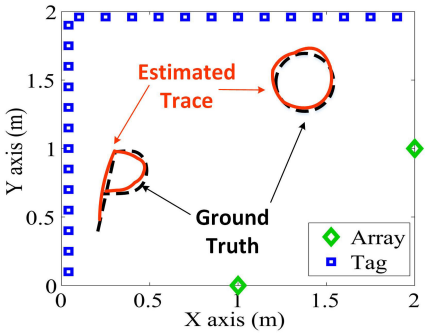

Figure 21: Passively track the fist's writing in the air.

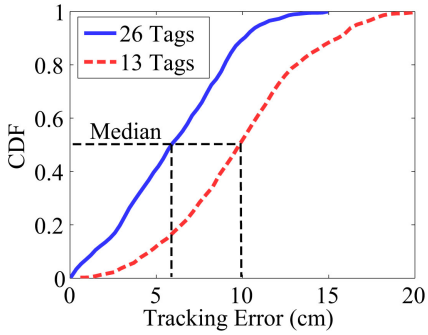

Figure 22: Fist tracking accuracy of D-Watch.

20 cm respectively. For each snapshot, we collect 30 data samples and the localization results are mapped into the heatmap, where the red dot represents the location estimate and the black cross indicates the ground truth. D-Watch localizes the three targets accurately with a maximum error of 17.2 cm when they are located sparsely, such as 130 cm and 50 cm apart. When the three targets are close to each other within 20 cm, the three targets have a tendency to merge into one on the heatmap and D-Watch can not localize each individual of them accurately. We believe with more number of antennas such as 16 and 64, finer AoA resolution can be achieved and we can further increase the accuracy and separability for multi-target localization.

6.8 Application Example: Tracking Fist in the Air for Virtual Screen Touch

One popular application in the research community recently is drawing in the air [39] or tracking the human's fine-grained gestures [12]. We briefly investigate the capability of D-Watch on these applications. We let a human user write the characters "P" and "O" along a pre-marked trajectory using his fist in the 2 m×2 m table area as shown in Fig. 21. The user moves his hand at a natural writing speed, i.e., about 0.5 m/s. Fig. 21 shows that the trajectory of the user's fist measured by D-Watch matches the ground truth quite well. To understand the tracking accuracy of D-Watch, we mark a set of continuous test points on the table. Fig. 22 shows that the median tracking error can be as small as 5.8 cm and 9.7 cm when 26 tags and 13 tags are employed respectively.

7. RELATED WORK

Device-free Localization. Early device-free localization works rely on visible light camera [28, 30] and infrared sensor [21, 19]. Camera-based methods heavily reply on lighting conditions and have severe privacy issue. Infrared-based methods have difficulties to penetrate the walls. On the other hand, low frequency RF waves can penetrate walls easily [7, 8, 55, 16] and RF infrastructures are widely available. Thus, there are growing interests in exploring RF signals for device-free localization. Among RF-based methods, most device-free localization systems are RSSI/CSI fingerprint-based [41, 42, 10, 11, 49, 43]. They translate the localization problem to a fingerprint matching problem while each location is associated with a unique RSSI or CSI fingerprint [49]. The feasibility has been demonstrated for different technologies including RFID [55, 18], Wi-Fi [33, 49] and ZigBee [57, 10]. However, fingerprint-based methods need a large amount of human efforts to acquire and update the fingerprint database. Changes in the environment, such as the movements of furniture, will change the fingerprints [51], causing mismatches between the database and the new measurements. D-Watch on the other hand, does not need any labor-

intensive training efforts, and only requires several baseline AoA measurements which can be carried out automatically without human interventions within seconds.

Recently, a lot of RSSI model-based device-free localization systems were proposed in order to reduce or even avoid the offline training efforts, such as RFID-based Tadar [55] and Twins [18] systems, Wi-Fi-based LiFS [44] and ACE [33] systems, ZigBee-based RTI [48] and RASS [57] systems, etc. The basic idea of these approaches is to model the wireless propagation channels mathematically and then estimate the target location from the distorted wireless signal. However, due to the complicated multipath situation in indoor environment, mathematical models do not fit well and the location accuracy is hence coarse. Also as the models focus on the LoS path, a dense transceiver deployment is usually needed to cover the area. Moreover, they require the prior knowledge of the locations of the transceivers, which are sometimes impractical. In contrast, D-Watch utilizes both the LoS path and the reflection paths for localization purpose, which significantly increases the coverage area and accuracy. The deployment density can thus be reduced, making it a promising candidate for large scale deployment. Further, D-Watch does not need to know the locations of the signal sources (such as the RFID tags or mobile devices) so the proposed system has a high flexibility for real life deployment.

Researchers also proposed some fine-grained device-free localization systems, such as Wi-Vi [8], Witrack [7], mtrack [47], etc. These systems though being able to achieve a high accuracy, require either dedicated signal (frequency modulated carrier wave, FMCW), specialized hardware (USRPs, WARP) or a very large bandwidth (60 GHz). Unlike these approaches, D-Watch is built on top of low cost COTS RFID devices and efficiently utilizes the "detrimental" multipaths to improve the coverage rate and localization accuracy.

Phase Calibration. Besides the wired phase calibration method introduced in ArrayTrack [51], some wireless phase calibration methods have also been proposed in Argos [37] and Phaser [17]. The method proposed in Argos can not be applied directly to our case as the RFID reader does not support transmission from one antenna on the reader to the other antennas. Also Argos requires all the transceivers to cooperate with each other for calibration, which interrupts the ongoing data transmissions. To overcome this limitation, Phaser is proposed and can carry out auto-calibration without interrupting the ongoing transmission. However, the calibration accuracy of Phaser is coarse. Our proposed calibration method not only achieves a much higher accuracy but also does not interrupt the ongoing data communication.

8. DISCUSSION

Deadzone problem: When a target does not block any path, it is in a "deadone" where the target can not be detected. In this case, D-Watch can utilize the mobility of a target to mitigate this problem. A human target moves continuously in space and the target can still be localized before and after entering into the "deadzone". These location information can then be utilized to estimate the target's current location when target is in the "deadzone". Moreover, there are rich multipaths in a typical indoor environment and the tags are very cheap so we can increase the number of tags to reduce the amount of deadzones. Thus, the probability of this extreme case is quite low in reality.

Mobility: Since the human target moves continuously, we can track the target by snapshots. In the indoor environment, the walking speed of a human is around 1–2 m/s. Note that the transmission interval of D-Watch is 0.1 s so the target moves only 10–20 cm in this short period which does not affect D-Watch's performance much. Also Doppler shift can be applied to estimate the target's walking speed to further improve the location accuracy.

Latency of D-Watch: The system latency includes the time to collect packets and the time to calculate the target location. We run our localization algorithm many times and the average processing time is 57 ms. 2–3 packets are employed for localization in D-Watch. The time taken to collect data packets depends on how frequently the packets are sent out. If the packet is sent out every 100 ms, the end-to-end system latency of our system is still well below 0.5 s.

9. CONCLUSION

D-Watch is the first device-free localization system that utilizes both the direct path and multipaths to provide decimeter-level localization accuracy without offline training. We propose a wireless phase calibration scheme to remove the random phase offsets at the radio front ends and a novel power MUSIC algorithm to accurately detect the angle information of the target. Comprehensive real-world experiments in different environments demonstrate the effectiveness of D-Watch. D-Watch can further localize multiple targets accurately which is a well known challenging problem in passive tracking. D-Watch outperforms the state-of-the-art systems and can be extended to work with other RF technologies and support other applications.

Acknowledgment

This work is supported by National Natural Science Foundation of China (61272461, 61572219, 61502192, 61572402, 61672428), Fundamental Research Funds for the Central Universities under Grant 2016JCTD118, and the Google fund to Jie Xiong at Singapore Management University. We also would like to thank the shepherd Swarun Kumar as well as the anonymous reviewers for their valuable feedback on this paper. Hongbo Jiang and Dingyi Fang are the corresponding authors.

10. REFERENCES

[1] Alien tags. www.alientechnology.com/tags/.

[2] Amazon, Inc. https://www.amazon.com/.

[3] Ans-900 rfid antenna. rf-links.com/newsite/pdf/ans-900.pdf.

[4] Epc gen2, epcglobal. www.gs1.org/epcglobal.

[5] Impinj, Inc. www.impinj.com/products/readers/speedway-revolution/.

[6] Q900f-900 rfid antenna. www.hrtantenna.com/en/products.

[7] F. Adib, Z. Kabelac, and D. Katabi. Multi-person localization via rf body reflections. In *Proc. Usenix NSDI*, pages 279–292, 2015.

[8] F. Adib and D. Katabi. See through walls with wifi! In *Proc. ACM SIGCOMM*, volume 43, pages 75–86, 2013.

[9] M. S. Bazaraa, H. D. Sherali, and C. M. Shetty. *Nonlinear programming: theory and algorithms*. John Wiley & Sons.

[10] L. Chang, X. Chen, D. Fang, J. Wang, T. Xing, C. Liu, and Z. Tang. Fale: Fine-grained device free localization that can adaptively work in different areas with little effort. *Acm Sigcomm Computer Communication Review*, 45(5):601–602, 2015.

[11] L. Chang, X. Chen, Y. Wang, D. Fang, J. Wang, T. Xing, and Z. Tang. Fitloc: Fine-grained and low-cost device-free localization for multiple targets over various areas. In *Proc. IEEE INFOCOM*, pages 151–159, 2016.

[12] B. Chen, V. Yenamandra, and K. Srinivasan. Tracking keystrokes using wireless signals. In *Proc. ACM Mobisys*, pages 31–44, 2015.

[13] B. Chen, Z. Zhou, and H. Yu. Understanding rfid counting protocols. *IEEE/ACM Trans. on Networking*, 24(1):312–327, 2016.

[14] R. Diamant, H. P. Tan, and L. Lampe. Los and nlos classification for underwater acoustic localization. *IEEE Trans. on Mobile Computing*, 13(2):311–323, 2014.

[15] A. EPCglobal Inc. Low level reader protocol, version 1.0. 1. 2007.

[16] M. Flores, U. Klarman, and A. Kuzmanovic. Wi-fm: Resolving neighborhood wireless network affairs by listening to music. In *Proc. IEEE ICNP*.

[17] J. Gjengset, J. Xiong, G. McPhillips, and K. Jamieson. Phaser: enabling phased array signal processing on commodity wifi access points. In *Proc. ACM MobiCom*, pages 153–164, 2014.

[18] J. Han, C. Qian, X. Wang, D. Ma, J. Zhao, P. Zhang, W. Xi, and Z. Jiang. Twins: Device-free object tracking using passive tags. In *Proc. IEEE INFOCOM*, pages 469–476, 2014.

[19] D. Hauschildt and N. Kirchhof. Advances in thermal infrared localization: Challenges and solutions. In *International Conference on Indoor Positioning and Indoor Navigation (IPIN)*, pages 1–8, 2010.

[20] P. Jain, J. Manweiler, and R. Roy Choudhury. Overlay: Practical mobile augmented reality. In *Proc. ACM Mobisys*, pages 331–344, 2015.

[21] J. Kemper and D. Hauschildt. Passive infrared localization with a probability hypothesis density filter. In *Proc. IEEE workshop on Positioning Navigation and Communication (WPNC)*, pages 68–76, 2010.

[22] M. Kotaru, K. Joshi, D. Bharadia, and S. Katti. Spotfi: Decimeter level localization using wifi. In *Proc. ACM SIGCOMM*, pages 269–282, 2015.

[23] S. Kumar, S. Gil, D. Katabi, and D. Rus. Accurate indoor localization with zero start-up cost. In *Proc. ACM MobiCom*, pages 483–494, 2014.

[24] T.-W. Kuo, K.-C. Lee, K. C.-J. Lin, and M.-J. Tsai. Leader-contention-based user matching for 802.11 multiuser mimo networks. *IEEE Trans. on Wireless Communications*, 13(8):4389–4400, 2014.

[25] L. Li, P. Hu, C. Peng, G. Shen, and F. Zhao. Epsilon: A visible light based positioning system. In *Proc. Usenix NSDI*, pages 331–343, 2014.

[26] T. Li, C. An, Z. Tian, A. T. Campbell, and X. Zhou. Human sensing using visible light communication. In *Proc. ACM MobiCom*, pages 331–344, 2015.

[27] X. Li, S. Li, D. Zhang, J. Xiong, Y. Wang, and H. Mei. Dynamic-music: accurate device-free indoor localization. In *Proc. ACM UbiComp*, pages 196–207, 2016.

[28] H. Ma, C. Zeng, and C. X. Ling. A reliable people counting system via multiple cameras. *ACM Trans. on Intelligent Systems and Technology*, 3(2):67–83, 2012.

[29] T. Mcconaghy, E. Vladislavleva, and R. Riolo. Genetic programming theory and practice 2010: An introduction. *Gecco Companion Publication Proceedings of Annual Genetic & Evolutionary Computation Conference*, 78(1):3015–3056, 2010.

[30] R. Mohedano, A. Cavallaro, and N. Garcĺła. Camera localization using trajectories and maps. *IEEE Trans. on Pattern Analysis & Machine Intelligence*, 36(4):684–697, 2014.

[31] F. M. Naini, J. Unnikrishnan, P. Thiran, and M. Vetterli. Where you are is who you are: User identification by matching statistics. *IEEE Trans. on Information Forensics & Security*, 11(2):358–372, 2016.

[32] S. J. Orfanidis. *Electromagnetic waves and antennas*. Rutgers University New Brunswick, NJ, 2002.

[33] I. Sabek, M. Youssef, and A. V. Vasilakos. Ace: An accurate and efficient multi-entity device-free wlan localization system. *IEEE Trans. on Mobile*

Computing, 14(2):261–273, 2015.

[34] R. O. Schmidt. Multiple emitter location and signal parameter estimation. *IEEE Trans. on Antennas and Propagation*, 34(3):276–280, 1986.

[35] R. O. Schmidt. Multiple emitter location and signal parameter estimation. *IEEE Trans. on Antennas and Propagation*, 34(3):276–280, 1986.

[36] T.-J. Shan, M. Wax, and T. Kailath. On spatial smoothing for direction-of-arrival estimation of coherent signals. *IEEE Trans. on Acoustics, Speech, and Signal Processing*, 33(4):806–811, 1985.

[37] C. Shepard, H. Yu, N. Anand, E. Li, T. Marzetta, R. Yang, and L. Zhong. Argos: Practical many-antenna base stations. In *Proc. ACM MobiCom*, pages 53–64, 2012.

[38] Y. Shu, K. G. Shin, T. He, and J. Chen. Last-mile navigation using smartphones. In *Proc. ACM MobiCom*, pages 512–524, 2015.

[39] L. Sun, S. Sen, D. Koutsonikolas, and K.-H. Kim. Widraw: Enabling hands-free drawing in the air on commodity wifi devices. In *Proc. ACM MobiCom*, pages 77–89, 2015.

[40] D. Vasisht, S. Kumar, and D. Katabi. Decimeter-level localization with a single wifi access point. In *Proc. Usenix NSDI*, pages 165–178, 2016.

[41] J. Wang, X. Chen, D. Fang, C. Q. Wu, Z. Yang, and T. Xing. Transferring compressive sensing based device-free localization across target diversity. *IEEE Trans. on Industrial Electronics*, 62(4):2397–2409, 2015.

[42] J. Wang, D. Fang, X. Chen, Z. Yang, T. Xing, and L. Cai. Lcs: Compressive sensing based device-free localization for multiple targets in sensor networks. In *Proc. IEEE INFOCOM*, pages 145–149, 2013.

[43] J. Wang, D. Fang, Z. Yang, H. Jiang, X. Chen, T. Xing, and L. Cai. E-hipa: An energy-efficient framework for high-precision multi-target adaptive device-free localization. *IEEE Trans. on Mobile Computing*, 12(5):1–12, 2016.

[44] J. Wang, H. Jiang, J. Xiong, K. Jamieson, X. Chen, D. Fang, and B. Xie. Lifs: Low human-effort, device-free localization with fine-grained subcarrier information. In *Proc. ACM MobiCom*, pages 243–256, 2016.

[45] J. Wang and D. Katabi. Dude, where's my card? rfid positioning that works with multipath and non-line of sight. In *Proc. ACM SIGCOMM*, volume 43, pages 51–62, 2013.

[46] J. Wang, D. Vasisht, and D. Katabi. Rf-idraw: virtual touch screen in the air using rf signals. In *Proc. ACM SIGCOMM*, volume 44, pages 235–246, 2014.

[47] T. Wei and X. Zhang. mtrack: High-precision passive tracking using millimeter wave radios. In *Proc. ACM MobiCom*, pages 117–129, 2015.

[48] J. Wilson and N. Patwari. See-through walls: Motion tracking using variance-based radio tomography networks. *IEEE Trans. on Mobile Computing*, 10(5):612–621, 2011.

[49] J. Xiao, K. Wu, Y. Yi, L. Wang, and L. M. Ni. Pilot: Passive device-free indoor localization using channel state information. In *Proc. IEEE international conference on Distributed computing systems (ICDCS)*, pages 236–245, 2013.

[50] J. Xiong and K. Jamieson. Towards fine-grained radio-based indoor location. In *Proc. ACM Workshop on Mobile Computing Systems & Applications*, pages 13–18, 2012.

[51] J. Xiong and K. Jamieson. Arraytrack: a fine-grained indoor location system. In *Proc. Usenix NSDI*, pages 71–84, 2013.

[52] J. Xiong, K. Jamieson, and K. Sundaresan. Synchronicity: pushing the envelope of fine-grained localization with distributed mimo. In *Proc. ACM Workshop on Hot Topics in Wireless*, pages 43–48, 2014.

[53] J. Xiong, K. Sundaresan, and K. Jamieson. Tonetrack: Leveraging frequency-agile radios for time-based indoor wireless localization. In *Proc. ACM MobiCom*, pages 537–549, 2015.

[54] C. Xu, B. Firner, R. S. Moore, Y. Zhang, W. Trappe, R. Howard, F. Zhang, and N. An. Scpl: indoor device-free multi-subject counting and localization using radio signal strength. In *Proc. ACM/IEEE IPSN*, pages 79–90, 2013.

[55] L. Yang, Q. Lin, X. Li, T. Liu, and Y. Liu. See through walls with cots rfid system! In *Proc. ACM MobiCom*, pages 1–12, 2015.

[56] S. Yun, Y.-C. Chen, and L. Qiu. Turning a mobile device into a mouse in the air. In *Proc. ACM Mobisys*, pages 15–29, 2015.

[57] D. Zhang, Y. Liu, X. Guo, and L. M. Ni. Rass: A real-time, accurate, and scalable system for tracking transceiver-free objects. *IEEE Trans. on Parallel and Distributed Systems*, 24(5):996–1008, 2013.

[58] Y. Zhu, Y. Zhu, B. Y. Zhao, and H. Zheng. Reusing 60ghz radios for mobile radar imaging. In *Proc. ACM MobiCom*, pages 103–116, 2015.